Applied Catalysis B: Environmental 210 (2017) 212–222

Contents lists available at ScienceDirect

Applied Catalysis B: Environmental

journal homepage: www.elsevier.com/locate/apcatb

Research paper

Hydrogen production from formic acid dehydrogenation over Pd/C catalysts: Effect of metal and support properties on the catalytic performance

Hyo-jin Jeon, Young-Min Chung*

Department of Nano & Chemical Engineering, Kunsan National University, 558 Daehak-ro, Kunsan, Jeollabuk-Do 573-701, Republic of Korea

ARTICLE INFO

Article history:
Received 2 February 2017
Received in revised form 22 March 2017
Accepted 28 March 2017
Available online 29 March 2017

Keywords:
Pd/C
Formic acid
Dehydrogenation
Hydrogen
Hydrogen storage

ABSTRACT

While formic acid dehydrogenation has become one of the most promising strategies for hydrogen storage, the crucial factors for realizing an efficient catalyst remain controversial. In this study, a range of Pd/C catalysts were systematically prepared by adopting either diverse metal deposition methods or different acid treatments, and the resulting catalysts were used for formic acid dehydrogenation under ambient conditions without additives. The volcano-type dependence of the activity on the Pd particle size, rate enhancement over Pd with smaller [111]/[200] ratios, and superior activity of Pd^0 or $Pd^0/Pd(OH)_2$ mixture to Pd^{2+} clearly indicate that not only the particle size but also the surface structure or electronic states of active metal would be of prime importance to promote the reaction. Moreover, another volcano relation between the activity and the pH of a reaction solution determined by the functional groups of an acid-treated support obviously suggests that the catalytic activity is very sensitive to pH, and that a neutral reaction solution is preferred to maximize the catalytic performance. The unprecedented critical effect of a support on the catalytic performance may be rationalized in terms of two factors: (i) recombination of the formate ion with a proton and/or delay of formic acid deprotonation by excess protons in an acidic solution; (ii) competitive adsorption between the formate and hydroxyl ions in a basic solution. Therefore, tuning the nature of a support to achieve a balance between the two competitive factors is important to enhance the catalytic performance.

1. Introduction

Hydrogen, which is one of the most essential reagents used in the refining and petrochemical industries, extends its importance as a promising energy carrier to satisfy the increasing demands for clean energy. However, a difficulty associated with the use of hydrogen as an energy carrier lies in the efficient production of hydrogen from cheap and abundant renewable sources, and its reversible storage without any safety concerns. In this context, organic hydrides, ammonia-borane, and formic acid have been extensively studied [1–4]. Among the potential candidates for hydrogen storage, formic acid appears to be superior because of its abundance, non-toxic nature, ease of hydrogen generation via dehydrogenation under ambient conditions, and easy storage via hydrogenation of captured CO_2 [5]. In particular, the ambient reaction temperature required for formic acid dehydrogenation renders formic acid more attractive for use as a hydrogen carrier in fuel cells designed for portable electronic appliances.

In line with the potential application of formic acid as a hydrogen carrier in fuel cell, the last decade witnessed the rejuvenation of the classical formic acid dehydrogenation in the presence of a number of homogeneous or heterogeneous catalysts under ambient conditions. However, intrinsic drawbacks for both homogeneous and heterogeneous catalysis encumber the commercial application of formic acid-based hydrogen storage. In a homogeneous system, the high activity of the catalyst for hydrogen generation at room temperature makes it possible to meet the requirement for mobile applications [6–8]. However, some severe problems such as difficult catalyst recovery, unstable nature of the catalysts, need for additives, and narrow pH range for the reaction remain to be solved [1]. In a heterogeneous system, on the other hand, unsatisfactory hydrogen generation rate, unfavorable coproduction of poisonous CO, and higher reaction temperature have been considered as stubborn difficulties.

Since Tsang and coworkers realized sufficiently active and selective Ag-Pd core-shell catalysts for the formic acid dehydrogenation

* Corresponding author.
E-mail address: ymchung@kunsan.ac.kr (Y.-M. Chung).

http://dx.doi.org/10.1016/j.apcatb.2017.03.070
0926-3373/

at room temperature [9], formic acid dehydrogenation over heterogeneous catalysts has drawn increasing attention. One of the key factors for elegant catalyst design is the precise control of metal nanoparticles and support integration [10], and a number of studies have focused on the tuning of active metals or the use of various supporting materials, or a combination of suitable active metal and support. For example, not only monometallic Pd [11–19] but also bi-/trimetallic Ag-Pd [20–26], Au-Pd [27,28], Pd-Ni-Ag [29], Cr-Au-Pd [30], Co-Au-Pd [31], Pd-MnO_x [32], Au-Pd-MnO_x [33], and Ag-Pd-MnO_x [34,35] systems with various metal ratios have been extensively studied. Moreover, a wide range of supports including carbon materials [11,13–17,25,28], metal oxides [18,19,32,33,35], polymer resins [20], and metal-organic frameworks [12,21,22,24,27,34] have been adopted and evaluated. Adopting their novel approaches such as non-noble metal sacrifice [36] and weakly-capping growth [37], Xu and coworkers also demonstrated that efficient prevention of active metal aggregation is advantageous to accelerate the reaction rate.

In spite of the rapidly increasing interest for formic acid dehydrogenation, it is difficult to find a consistent trend for the factors affecting the catalytic performance; therefore, the strategy for realizing an efficient catalyst is still controversial. For instance, the composition of a Pd/C catalyst is very simple, however, to the best of our knowledge, there are limited studies in this regard [11,13,14,17]. Further, a systematic study on the effect of catalyst preparation methods on the performance of the formic acid dehydrogenation has not been reported. In the present study, a range of Pd/C catalysts were systematically prepared using different methods, and the effect of their physicochemical properties on the efficiency of formic acid dehydrogenation was elucidated.

2. Experimental

2.1. Chemicals

Activated carbon and polyvinylpyrrolidone (PVP, mol. wt. 40,000) were purchased from Sigma-Aldrich. Palladium (II) acetate (>99.95%), palladium chloride (99.9%), and sodium carbonate (99.5%) were purchased from Strem-Chemicals, Alfa Aesar, and Kanto Chemical, respectively. Acetone (99.5%), diethylene glycol (99%), dioxane (99.5%), ethanol (99.5%), formic acid (99%), hydrochloric acid (35–37%), methanol (99.5%), sodium bicarbonate (99%), and sodium hydroxide (98%) were supplied from Samchun Chemicals in South Korea. Pd-doped sulfonic acid-bound polymer resin (K2624) was obtained from Lanxess (Germany). All chemicals were used as received without further purification.

2.2. Catalyst preparation

2.2.1. NP method

The colloidal Pd nanoparticles were prepared by polyol method using palladium (II) acetate (Pd precursor), PVP (nanoparticle stabilizing agent), and ethylene glycol (solvent and reducing agent) according to the procedure reported elsewhere [17,38]. For nanoparticle synthesis, two different solutions were prepared in advance. The first solution was prepared by dissolving PVP (10 mmol) in ethylene glycol (120 ml) at 353 K for 2 h with stirring. After cooling to 273 K, 1 M NaOH (3 ml) solution was added to adjust pH, and the resulting mixture was stirred for 20 min. The second solution was prepared by dissolving $Pd(OAc)_2$ in dioxane (50 ml) at room temperature. After adding the second metal precursor solution to the first PVP solution, the mixed solution was heated up to 373 K and kept at this temperature for 2 h under vigorous stirring. During the reduction process, the bright orange color of the solution gradually turned into dark brown, which suggested the reduction of Pd^{2+} to Pd^0. After completing the reduction, the colloidal solution was cooled down to room temperature, and the resulting Pd nanoparticles were purified with acetone. Addition of acetone under vigorous stirring not only made residual PVP transfer to acetone phase but also caused flocculation of the Pd nanoparticles. The purified nanoparticles were redispersed in methanol (200 ml) for further use. The colloidal Pd nanoparticles was impregnated on activated carbon by simply adsorption method. Activated carbon was suspended in methanol solution in which Pd nanoparticles were dispersed (intake 5 wt%). After stirred for 72 h, the catalyst was dried at 333 K under vacuum to remove methanol, washed several times with ethanol, and dried overnight at 333 K. The catalyst prepared by adsorption of the "ready-made" nanoparticles on activated carbon was denoted as **NP**.

2.2.2. AR method

Activated carbon suspended in deionized water was mixed with metal precursor solution (0.034 g of $PdCl_2$ dissolved in 5 ml of 0.2 M HCl), and the resulting solution was stirred at room temperature for 2 h. After then, reduction was carried out by bubbling hydrogen (20 ml/min) at 353 K for 2 h under vigorous stirring. Cooled down to room temperature, the ready-made catalyst was filtered, washed with deionized water several times, and dried overnight at 393 K. The catalyst prepared by the metal precursor adsorption – reduction method was designated as **AR**.

2.2.3. ADR method

The preparation method was similar with **AR** except for the use of NaOH for the formation of palladium hydroxide ($Pd(OH)_2$). After impregnation of Pd precursor to activated carbon and heating up to 393 K, the suspension was adjusted to pH 12 by dropping 0.5 M NaOH solution, and was additionally stirred for 2 h. After then, same reduction and purification procedures were performed as that of **AR** case. The resulting catalyst prepared by the adsorption – deposition – reduction method was referred to **ADR**.

2.2.4. IR method

For the activated carbon suspended in 1 M sodium carbonate (3.8 ml) solution, metal precursor solution was poured, and the resulting mixture was additionally stirred for 2 h. After reduction at 353 K with hydrogen (20 ml/min) for 2 h, the catalyst was purified as same as **AR** case. The catalyst prepared by the ion-exchange – reduction method was denoted as **IR**.

2.2.5. IDR method

In this method, activated carbon was also pre-treated with sodium carbonate. However, reduction was carried out at pH 12 by the addition of NaOH after impregnation as same as that of **IR**. The catalyst prepared by the ion-exchange – deposition – reduction method was designated as **IDR**.

2.2.6. SR method

1 M sodium carbonate was added to metal precursor solution, and the resulting mixture was stirred at room temperature for 2 h. The *in-situ* made colloidal Pd sols were adsorbed on activated carbon at room temperature, subsequently reduced with hydrogen at 353 K, and purified. The catalyst prepared by the sol formation – reduction method was called as **SR**.

2.2.7. SDR method

The catalyst preparation was carried out in a similar manner with that of **SR** except for the use of NaOH for the formation of palladium hydroxide ($Pd(OH)_2$). After impregnation was finished, pH of the solution was adjusted to 12, and reduction was performed with hydrogen at 353 K. The catalyst prepared by the sol formation – deposition – reduction method was designated as **SDR**.

Acid treatment of activated carbon: Activated carbon was refluxed in an acid solution such as 1 wt% HNO_3, 10 wt% HNO_3, or 10 wt% HNO_3/10 wt% H_2O_2 for 6 h to increase and/or modify the oxygen-containing groups on the activated carbon surface. The acid-treated activated carbon was washed with distilled water thoroughly, and dried in an oven at 383 K for 12 h.

2.3. Catalyst characterization

X-ray powder diffraction (XRD) anlaysis was carried out on a Rigaku diffractometer using CuKα (λ = 1.54 Å) radiation at 0.5°/min. The textual properties including specific surface area, pore volume, and pore diameter of catalysts were determined by N_2 adsorption using a BELSORP-Max (BEL, Japan) at 77 K. Prior to adsorption, samples were degassed under vacuum conditions at 423 K overnight. Binding energies of Pd in the catalyst and oxygen/carbon atomic ratio of acid-treated activated carbons were measured using X-ray photoelectron spectroscopy (MultiLab 2000, Thermo VG Scientific, UK, England). Data were acquired with a pass energy of 30 eV, a step increment of 0.1 eV, and an Al anode. XPS peak positions are referenced to the carbon (1 s) peak at 284.6 eV. Actual Pd content on activated carbon was determined by ICP-AES analysis using a Perkin-Elmer OPTIMA 7300 DV (Norwalk, CT, USA). Pd nanoparticle size distribution was determined using the images obtained from transmission electron microscopy (TEM) analysis (Philips, Tecnai G2 F30, Hillsboro, OR, USA).

The approximate distribution of different oxygen-containing groups on an acid-treated activated carbon surface was analyzed by titration, temperature-programmed desorption-mass spectrometry (TPD-Mass), and diffuse reflectance infrared Fourier transform spectroscopy (DRIFTS-IR). Titration was carried out based on Boehm's method using three reagents such as sodium carbonate, sodium bicarbonate, and sodium hydroxide [39]. Temperature-dependent gas evolutions of acid-treated activated carbons were monitored by TPD-Mass (BEL-CAT-Mass). Before experiment, samples were dried in a helium flow of 100 ml/min at 373 K for 2 h. The temperature of the samples was increased to 1273 K at a ramping rate of 5 K/min, and the decomposed gases were detected using the mass spectrometer. DRIFT spectra of acid-treated activated carbon supports were recorded by using FT-IR spectrometer (Nicolet iS50 with DTGS detector) equipped with diffuse IR chamber (Pike Technology).

2.4. Formic acid dehydrogenation

Formic acid dehydrogenation was carried out in a 100 ml three-necked round flask with water jacket. Before use, all catalysts were dried at 393 K for 4 h under vacuum condition. In a typical run, a reactor containing predetermined amount of catalyst and water (15 ml) was connected to gas burette, pressure-equalizing funnel containing formic acid (5 ml), and Ar gas line. Pd to formic acid molar ratio was maintained as 0.004. Before performing an activity test, the reaction medium was magnetically stirred for 30 min to achieve thermal equilibrium under inert condition. A reaction was initiated by injecting the formic acid in the connected pressure-equalizing funnel to the reaction medium under vigorous stirring. After then, the volume of the evolved gas was monitored by recording the displacement of water in the gas burette. The reaction temperature was precisely maintained by using water circulator connected to the reactor (typically 323 K). The released gas during a reaction was collected, and analyzed by Agilent 6890 Gas Chromatography equipped with Carboxen-1010 Plot capillary column and TCD/methanizer-FID detector.

Table 1
Catalyst preparation methods.

Indexing	Preparation method
NP	Adsorption of 'ready-made' nanoparticles
AR	Metal precursor adsorption – Reduction
ADR	Metal precursor adsorption – Deposition – Reduction
IR	Metal precursor ion exchange – Reduction
IDR	Metal precursor ion exchange – Deposition – Reduction
SR	'In-situ' metal sol formation – Reduction
SDR	'In-situ' metal sol formation – Deposition – Reduction

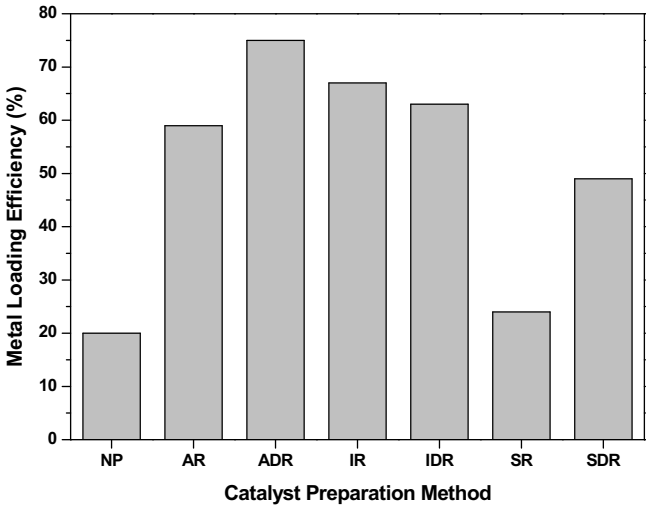

Fig. 1. Changes in the Pd metal loading efficiency depending on the catalyst preparation methods (metal loading efficiency (%) = actual Pd/intake Pd x 100).

3. Results and discussion

3.1. Preparation of Pd/C catalysts by different metal deposition methods, and their characterization

To investigate the effect of metal deposition methods on the catalytic performance of Pd/C for formic acid dehydrogenation, seven types of catalysts were prepared; the detailed preparation methods are listed in Table 1. As shown in Fig. 1, the amount of Pd impregnated on activated carbon was largely affected by the metal deposition method. In the case of the sol-immobilization method, such as **NP** (Pd^0 nanoparticles), **SR** (polynuclear hydroxopalladium complexes), or **SDR** ($Pd(OH)_2$ sols), the metal loading efficiency was unsatisfactory (<49%), regardless of the use of a stabilizing ligand. On the other hand, when the metal precursor ($PdCl_4^{2-}$) was first adsorbed (**AR**, **ADR**) or ion-exchanged (**IR**, **IDR**), over 60% of Pd was supported, and the metal loading efficiency was as high as 75% in the case of **ADR**. These facts indicate that the adsorption strength of the "ready-made" sols is lower than that of the Pd ion. In addition, the observed large difference in the metal loading efficiency between **SR** and **SDR** may be ascribed to the different sol formation, which suggests that the smaller $Pd(OH)_2$ sols are superior to polynuclear hydroxopalladium complexes in terms of immobilization on the tortuous activated carbon surface.

Fig. 2 shows the representative transmission electron microscopy (TEM) images of the Pd/C catalysts. The Pd nanoparticle size was strongly dependent on the preparation methods, and reduction under high pH conditions resulted in the formation of smaller metal nanoparticles, regardless of the order of addition. For example, while relatively larger and polydisperse nanoparticles (9.4 ± 1.4 nm) were produced by the **AR** method, the addition of NaOH in the **ADR** method made it possible to considerably reduce the particle size and improve the nanoparticle distribution

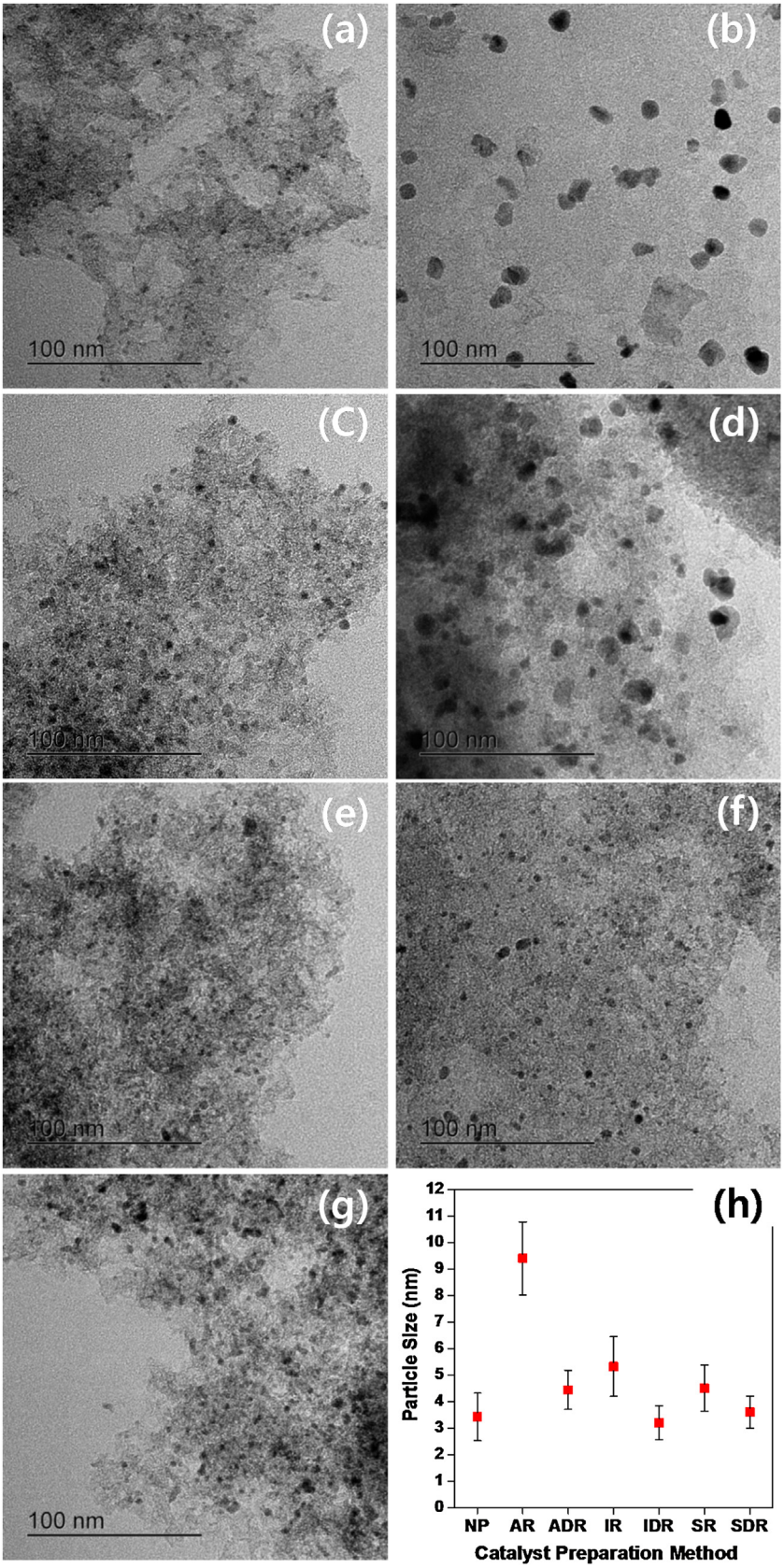

Fig. 2. TEM images of Pd/C catalysts and their Pd nanoparticle size distributions; (a) NP, (b) AR, (c) ADR, (d) IR, (e) IDR, (f) SR, (g) SDR, and (h) nanoparticle size distributions.

(4.4 ± 0.7 nm). The beneficial effect of NaOH in improving nanoparticle distribution was also observed in the **IDR** and **SDR** methods. These facts clearly imply that the reduction of mononuclear $Pd(OH)_2$ formed at high pH (>10) [40] is more advantageous over

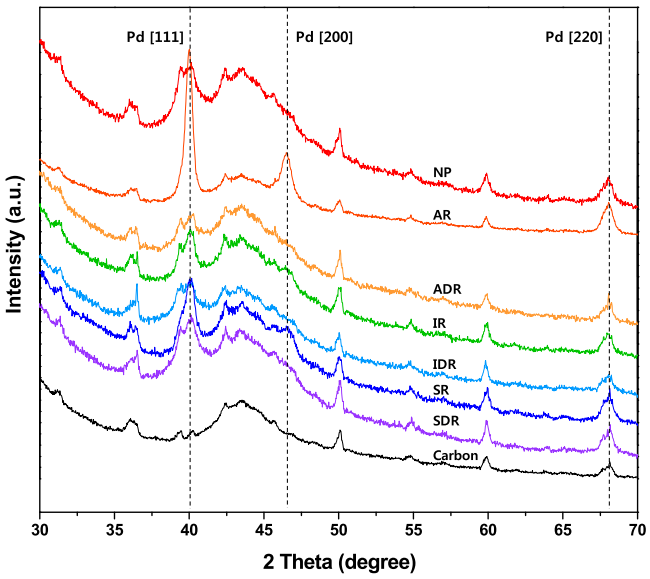

Fig. 3. XRD patterns of Pd/C catalysts prepared by different metal deposition methods.

that of Pd metal ions ($PdCl_4^{2-}$) or polynuclear hydroxopalladium complexes for obtaining smaller, monodisperse Pd nanoparticles.

The XRD patterns of the Pd/C catalysts are presented in Fig. 3. Except for **AR**, in which a large particle size is observed, neither the metal deposition method nor the palladium content had any appreciable influence on the crystallinity of Pd. However, the [111]/[200] ratio of the Pd crystallites was significantly affected by the preparation method, as shown in Table 2. Irrespective of the order of addition, the Pd^0 crystallites produced at high pH (~12) showed higher [111]/[200] ratio compared to their corresponding counterparts reduced at relatively lower pH. The [111]/[200] ratio in the case of **ADR**, **IDR**, and **SDR** is 4.4, 2.2, and 3.3 times higher than those for **AR**, **IR**, and **SR**, respectively. The existence of the [220] phase of the Pd crystallite could not be confirmed because the characteristic diffraction peak $2\theta = \sim 68^\circ$ overlapped with that of activated carbon.

To investigate the electronic states of Pd, X-ray photoelectron spectroscopy analysis was performed; the Pd 3d XPS spectra of Pd/C catalysts together with their deconvoluted chemical states are presented in Fig. 4. Pd existed in 2–3 types of electronic states, which varied with respect to the preparation method adopted. Reduced Pd peaks for the Pd($3d_{5/2}$) and Pd($3d_{3/2}$) spin–orbit doublet at approximately 335.6 and 340.8 eV [41] were observed for all samples. However, the XPS peaks observed around 337.8 (Pd^{2+} $3d_{5/2}$) and 342.8 eV (Pd^{2+} $3d_{3/2}$) implied that complete reduction was hardly achievable, regardless of the preparation method used. The presence of characteristic peaks ascribed to PdO (~336.4 and ~341.8 eV) [42] for the Pd/C catalysts prepared by the **ADR**, **IDR**, and **SDR** methods suggested the formation of $Pd(OH)_2$ upon the addition of NaOH.

Table 2
Effect of preparation methods on the phase ratio of Pd.

Preparation method	[111]	[200]	[111]/[200]	TOF (h^{-1})
NP	3901	178	21.9	38
AR	10165	3479	2.9	13
ADR	1736	135	12.9	75
IR	2474	566	4.4	87
IDR	1636	168	9.7	59
SR	3475	260	13.4	79
SDR	3475	79	43.9	57

3.2. Effect of metal deposition methods on the catalytic performance

Formic acid dehydrogenation was carried out at 323 K using the as-prepared Pd/C catalysts, and the reaction progress was monitored by quantifying the displacement of water in the gas burette. Fig. 5 shows the plots of the evolved gas ($CO_2 + H_2$) generated *versus* reaction time during the dehydrogenation of formic acid over a range of Pd/C catalysts. The catalytic performance was greatly dependent on the preparation methods; the Pd/C catalyst prepared by the **IR** method showed the best catalyst performance, with the initial turnover frequency (TOF) as high as 87 h^{-1}. Fig. 6 presents the dependence of the TOF on the particle size of Pd, which clearly shows that the Pd nanoparticle size has marked effect on the reaction performance of a catalyst. The volcano-type relationship strongly suggests that controlling the particle size of Pd is of prime importance to enhance the catalytic activity. Yamashita and coworkers also observed a similar volcano-type dependence of the Pd particle size on the TOF, and reported that the optimal particle size is approximately 3.9 nm [17]. In our study, however, a similar particle size (3.4 ± 0.9 nm) obtained by the immobilization of "ready-made" **NP** showed moderate catalytic performance, and larger particle size was superior to obtain higher TOF.

Moreover, the use of NaOH during catalyst preparation largely affected not only the TOF but also the total formic acid conversion. The TOF and total conversion in the case of the **IR** were 1.5 and 1.8 times higher than those for the **IDR** reduced at relatively higher pH. Similar reduction in the catalytic performance of **SDR** compared to **SR** was also investigated. These results suggest that besides the particle size, other features of Pd may also exert significant effects on the catalytic performance. In the case of **ADR**, the poor activity of **AR** was greatly improved by the addition of NaOH. The formation of smaller Pd nanoparticle may offset the adverse effects caused by the use of NaOH.

In addition to the optimal Pd nanoparticle sizes, the enhanced catalytic performance of **IR** and **SR** compared to those of their analogues such as **IDR** and **SDR** may be explained in terms of the difference in the surface structure of Pd induced by the treatment with NaOH during catalyst preparation. It has been reported that formic acid oxidation is a surface-sensitive reaction and that the [100] phase is more active than the [111] phase [43,44]. In this context, it is assumed that the increase in the Pd [200] phase of **IR** and **SR** may result in the enhancement of catalytic performance. Because the reaction paths for the formation of CO and CO_2 are strongly affected by the surface structure of the metal [45,46], it is also plausible that the difference in the total conversion between **IR** (or **SR**) and **IDR** (or **SDR**) may be attributed from the difference in CO formation with respect to the catalyst used. While we attempted to analyze the evolved gases several times to elucidate the hypothesis, CO was not detected from all samples.

Considering that there exist different concentrations of metallic, oxidized, and reduced Pd species in a single metal domain, as observed by XPS experiments, it is reasonable that the electronic states of Pd may be another important factor affecting the catalytic performance. In this regard, a range of catalysts with different electronic states were prepared and tested to elucidate the influence of electronic states of Pd on the catalytic performance. Indeed, it was found that the oxidation state of Pd played a very important role in determining its catalytic activity. As shown in Fig. 7, the Pd^{2+} ion was ineffective in promoting formic acid dehydrogenation. The slightly better activity of Pd^{2+}/C than that of Pd^{2+}/resin may be due to the presence of Pd^0, which possibly resulted from the reduction of Pd ions by the activated carbon support. While a single isolated Pd^{2+} cation on N-doped carbon has been reported to show good activity for gas-phase formic acid dehydrogenation [47], the

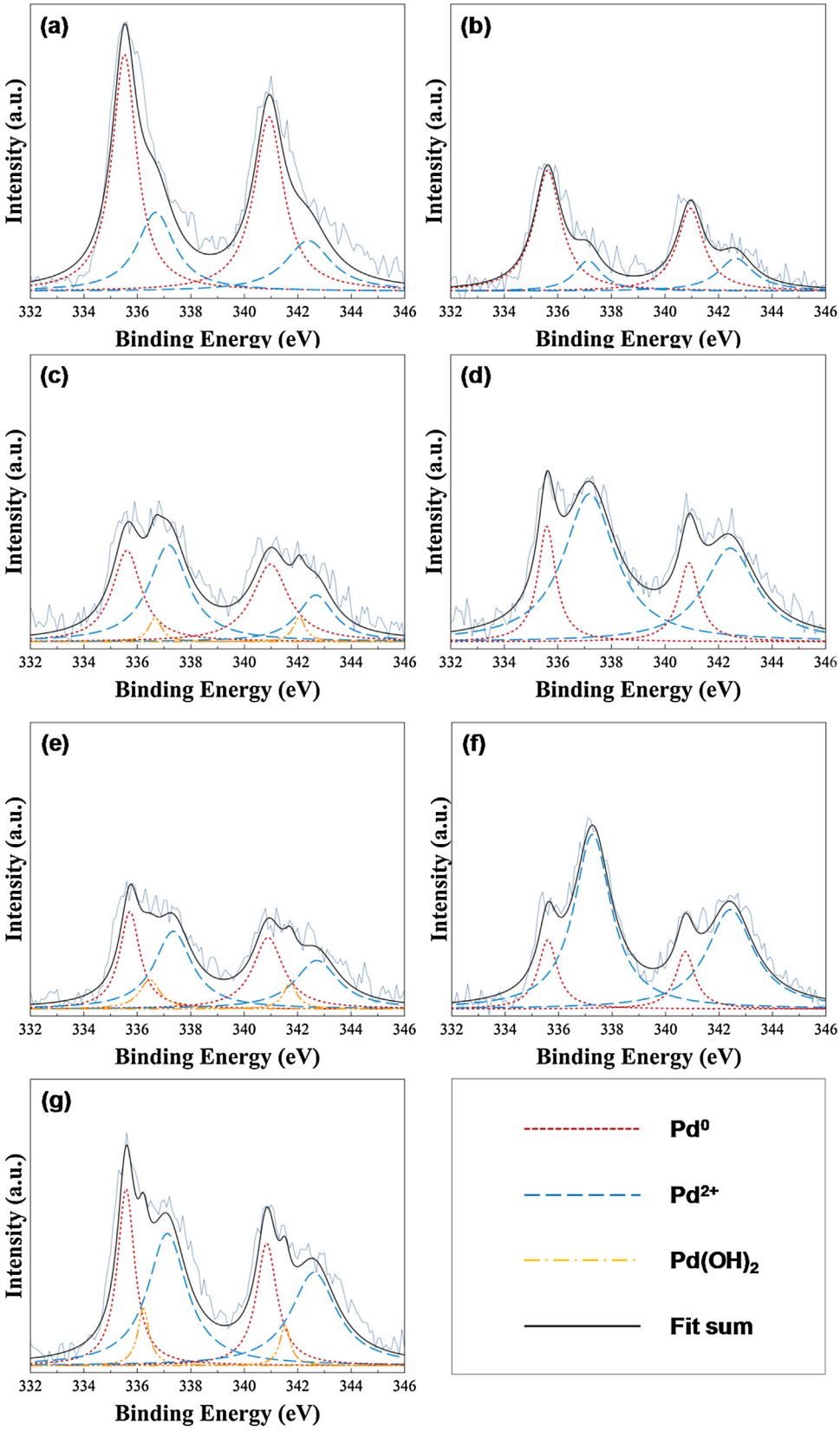

Fig. 4. Pd 3d XPS spectra (a) NP, (b) AR, (c) ADR, (d) IR, (e) IDR, (f) SR, and (g) SDR.

Pd^{2+} ion showed inferior catalytic performance in the liquid-phase reaction.

The enhanced catalytic performances of Pd^0/C and $Pd(OH)_2$/C may be clearly ascribed to the formation smaller Pd nanoparticles by the addition of NaOH during catalyst preparation. However, there is little difference in the Pd particle size between the oxidized and reduced catalysts, which strongly suggests that the electronic states of Pd may have a crucial role in promoting the reaction. In

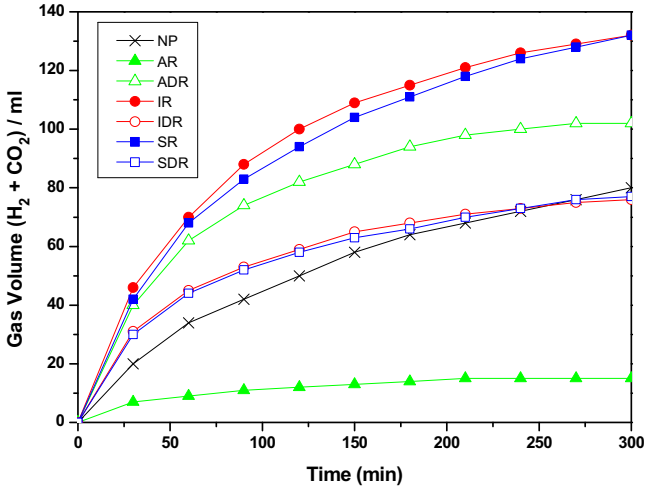

Fig. 5. Volume of the generated gas ($CO_2 + H_2$) versus time for the formic acid dehydrogenation over Pd/C catalysts prepared by different metal deposition methods.

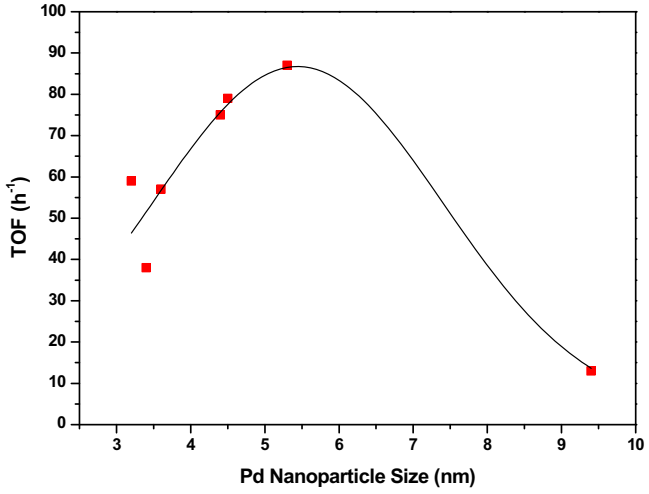

Fig. 6. The dependence of TOF on the Pd nanoparticle size.

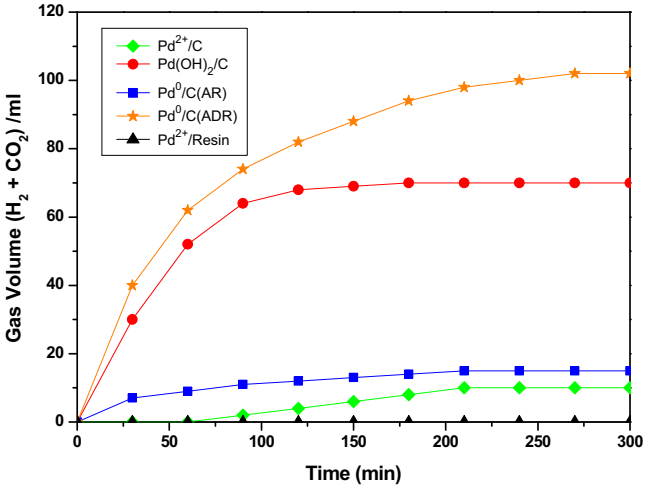

Fig. 7. Effect of the oxidation state of Pd on the catalytic performance of Pd/C for the formic acid dehydrogenation.

Table 3
Textual properties of acid-treated activated carbon supports.

Treatment	Surface area (m^2/g)	Pore volume (cm^3/g)	Pore diameter (nm)
Untreated	953	0.92	3.8
1 wt% HNO_3	1004	0.91	3.6
10 wt% HNO_3	960	0.81	3.4
10 wt% HNO_3 + 10 wt% H_2O_2	1012	0.85	3.4

the case of the $Pd(OH)_2/C$ catalysts, the oxidized $Pd(OH)_2$ species may act as Lewis acid sites that show strong affinity for the oxygen group of the formate ions and thus accelerate the adsorption of formate ions. The best reaction performance of Pd^0/C including both oxidized and reduced Pd species may be rationalized in terms of the following three aspects: (i) the reduced species is superior to the oxidized species in promoting the reaction, (ii) the formate ions adsorbed on $Pd(OH)_2$ move to nearby Pd^0 sites, where they can be more easily converted, and (iii) $Pd(OH)_2$ renders the Pd^0 sites more active by attracting the electrons of Pd^0. Recently, it was also reported that the electronic states of the metal markedly affected the reaction performance of ammonia borane decomposition, and an optimal proportion of metallic/oxidized metal species is critical to accelerate the decomposition rate [48,49]. It is also interesting that the total evolved gas volume of the Pearlman type catalyst ($Pd(OH)_2/C$) was considerably smaller than that of Pd^0/C, which suggests that the electronic status of Pd affected not only on the TOF but also on the catalyst stability. The effects of the phase ratios and electronic states of Pd on the catalytic performance strongly indicate that formic acid decomposition is also a surface-sensitive reaction, similar to formic acid oxidation [43,44].

3.3. Preparation and characterization of acid-treated activated carbon support

To investigate the effect of the surface nature of activated carbon on the reaction performance of the Pd/C catalyst, three types of acid-treated activated carbons were prepared, and their physicochemical properties were characterized. The changes in the textual properties of the acid-treated activated carbon are summarized in Table 3. The analysis shows that acid-treatments have little impact on the textual properties of activated carbon and that only the pore diameter and pore volume were slightly reduced in the case of 10 wt% HNO_3 treatment.

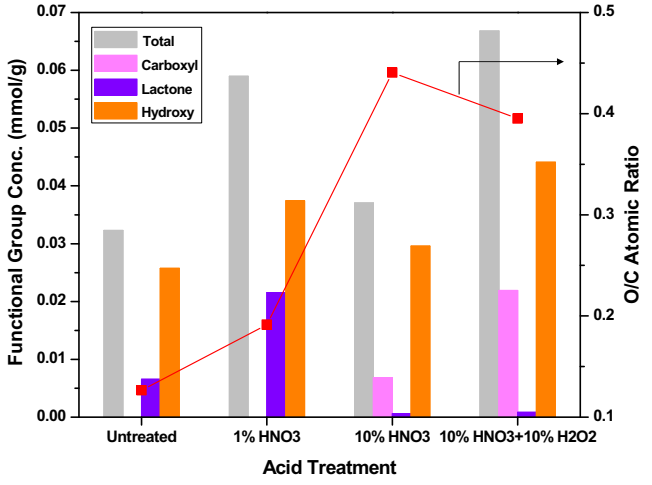

Fig. 8. Surface functional group distributions and O/C atomic ratio of acid-treated activated carbons.

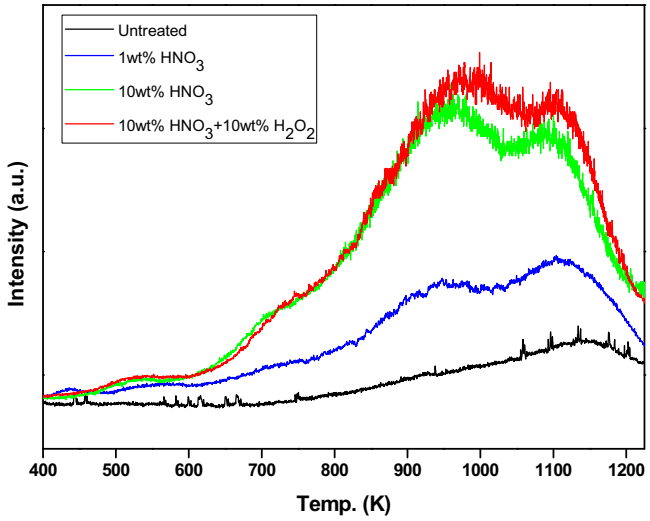

Fig. 9. Temperature-dependent CO evolution of acid-treated activated carbons monitored by temperature-programmed desorption-mass spectrometry.

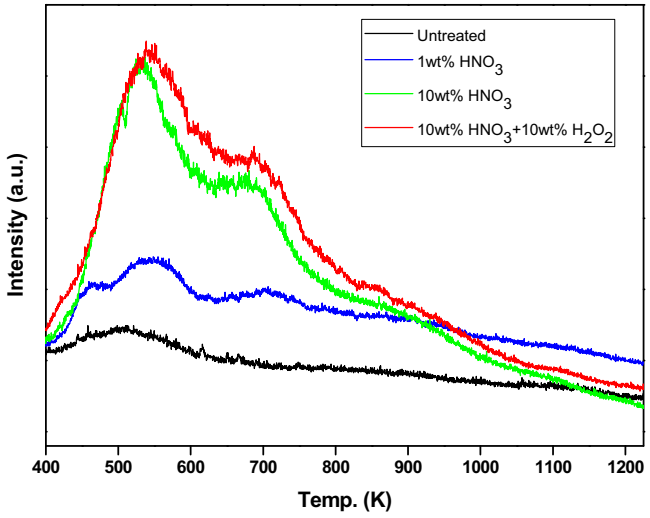

Fig. 10. Temperature-dependent CO_2 evolution of acid-treated activated carbons monitored by temperature-programmed desorption-mass spectrometry.

Fig. 8 presents the distribution of the surface oxygen-containing functional groups and O/C atomic ratio of activated carbon, as determined by chemical titration and XPS analysis, respectively. Titration experiments indicated that the nature of the oxygen-containing functional groups and their concentration on the activated carbon surface were largely affected by the acid treatment conditions. While lactone groups were observed from the untreated and the 1 wt% nitric acid treated samples, carboxyl groups were newly introduced in the case of 10 wt% nitric acid treatment at the expense of the reduction in the lactone groups. The hydroxyl group also existed in different concentrations, regardless of the acid treatment conditions. The higher O/C atomic ratio for the 10 wt% nitric acid treated activated carbons suggests the introduction of a larger amount of oxygen groups. Considering that XPS analyses reveals the amount of oxygen in the outer layer (2–3 nm) of activated carbon [50] and titration gives information about the amount of accessible surface oxygen groups, the relatively smaller amount of oxygen groups on the 10 wt% nitric acid treated activated carbon implies that the amount of accessible oxygen groups is different from the actual oxygen group concentration on the surface.

To assess the total oxygen content in the activated carbon domain, TPD-mass experiments were carried out; the temperature-dependent CO and CO_2 evolutions are presented in Figs. 9 and 10. The two distinct peaks with CO evolution around 900–1030 K and 1050–1150 K are ascribed to phenol, ether, and carbonyl structures. Carboxylic acids are responsible for the low-temperature peak (480–750 K) for CO_2 evolution, while the high-temperature shoulder observed around 900 K may be attributed to carboxylic anhydrides and lactones [51,52].

DRIFTS-IR analysis was also performed to investigate the changes in the surface functional groups with respect to different acid treatments. As shown in Fig. 11, the carbonyl (C=O) stretching band at ~1800 cm^{-1} is attributed to carboxylic acid or anhydride groups. The broad band from 1200 to 1450 cm^{-1} may be attributed to C=O stretching in the carboxylic acid and lactone, and to O—H bending. The peak at ~1600 cm^{-1} is due to the overlap between polyaromatic C=C stretching band and the peak resulting from the highly conjugated carbonyl and/or quinone groups [53,54]. The information about the surface functional groups obtained from the DRIFTS-IR analysis is closely consistent with that obtained from the titration, XPS, and TPD-mass experiments.

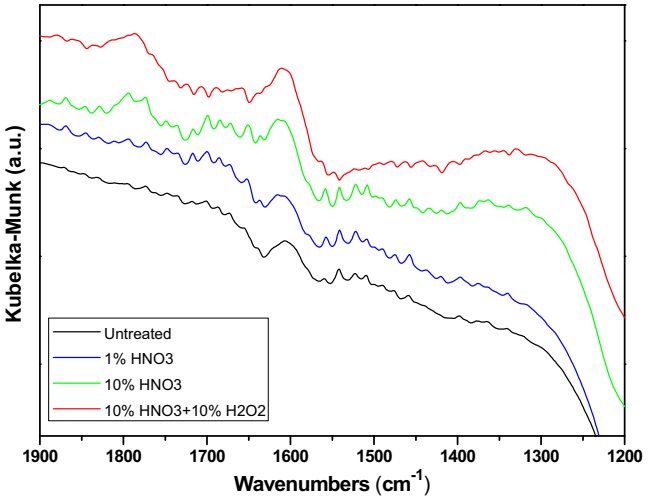

Fig. 11. DRIFTS-IR spectroscopy of acid-treated activated carbons.

3.4. Effect of acid treatment of support on the catalytic performance

To evaluate the effect of acid treatment of the activated carbon support on the catalytic performance, acid-treated Pd/C catalysts were prepared by the **IR** method. The TEM images of the four types of Pd/C catalysts shown in Fig. 12 indicate that an increase in the number of oxygen groups on the support due to the acid treatment resulted in the formation of smaller Pd nanoparticles. In particular, the average Pd nanoparticle size was 3.5 nm in the case of the Pd/C catalyst treated with 1 wt% nitric acid. This result implies that the particle size distribution is affected not only by the metal deposition method chosen but also by the surface nature of the support.

Formic acid dehydrogenations over a range of acid-treated Pd/C catalysts were carried out; the reaction profiles are presented in Fig. 13. The catalytic performance strongly depended on the surface feature of the support as well, and the best performance was obtained in the presence of the Pd/C catalyst treated with 1 wt% nitric acid. As already shown in Fig. 6, the TOF exhibited a volcano-type relation with the Pd nanoparticle size, and the optimal nanoparticle size was approximately 5.5 nm. In this context, one may expect the different performances of the acid-treated Pd/C catalysts to also be ascribed to the different Pd nanoparticle sizes.

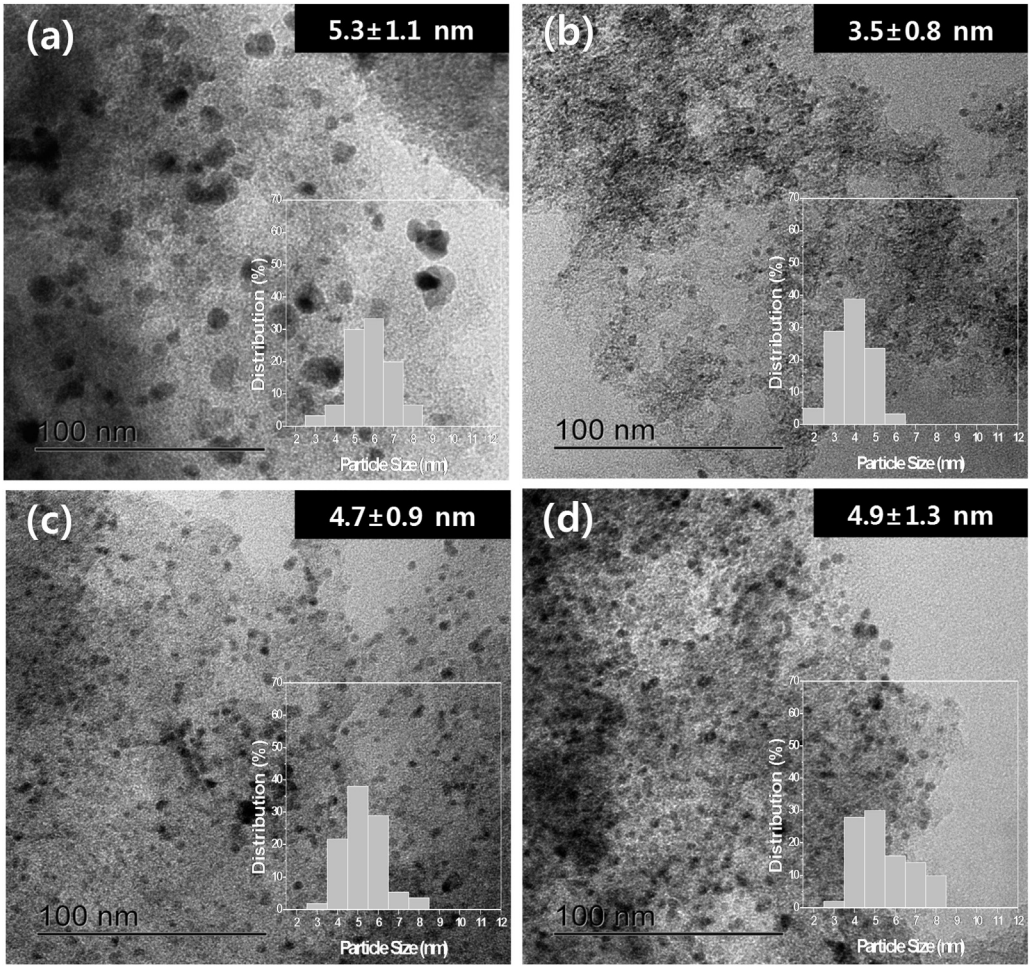

Fig. 12. TEM images of acid-treated Pd/C catalysts and their Pd nanoparticle size distributions; (a) untreated, (b) 1 wt% HNO_3, (c) 10 wt% HNO_3, and (d) 10 wt% HNO_3 + 10 wt% H_2O_2.

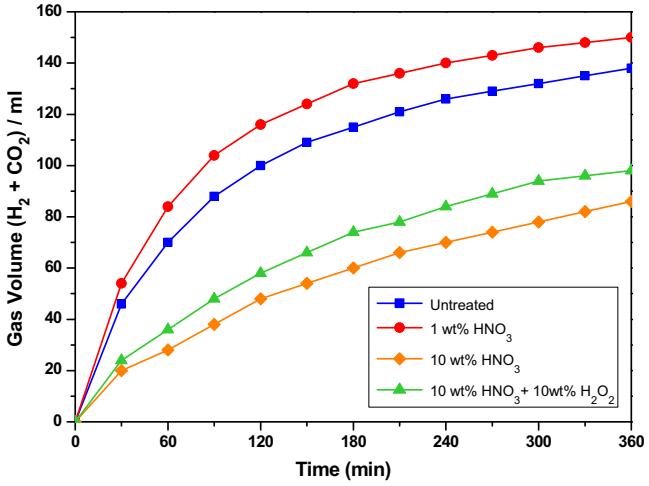

Fig. 13. Volume of the generated gas (CO_2 + H_2) versus time for the formic acid dehydrogenation over acid-treated Pd/C catalysts.

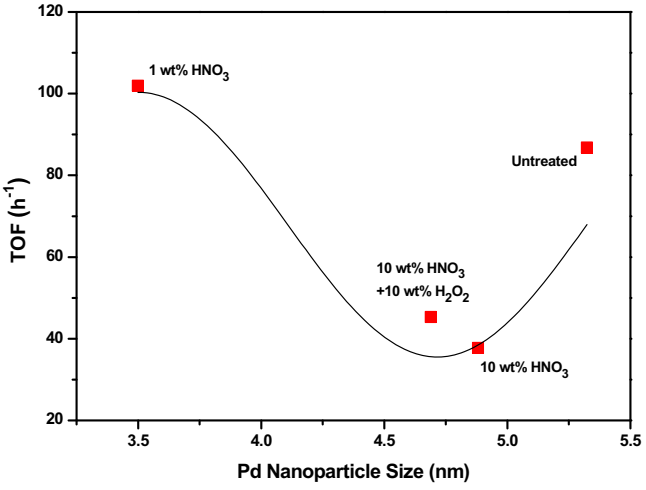

Fig. 14. The dependence of TOF on the Pd nanoparticle size of acid-treated Pd/C catalysts.

However, the entirely different or rather reversed relation between the TOF and the Pd nanoparticle size of the acid-treated Pd/C catalysts described in Fig. 14 strongly implies that it is no longer sufficient to rationalize the different catalytic activities in terms of the different Pd nanoparticle size if the surface characteristics changed upon acid treatment. The effect of the structural and electronic states of Pd on the catalytic activity can be excluded because there is little difference in the structural and electronic states of Pd between the acid-treated Pd/C catalysts.

To clarify the influence of the surface properties of the support on the catalytic activity, the pH of the reaction solutions containing the acid-treated Pd/C catalysts was measured. The results showed

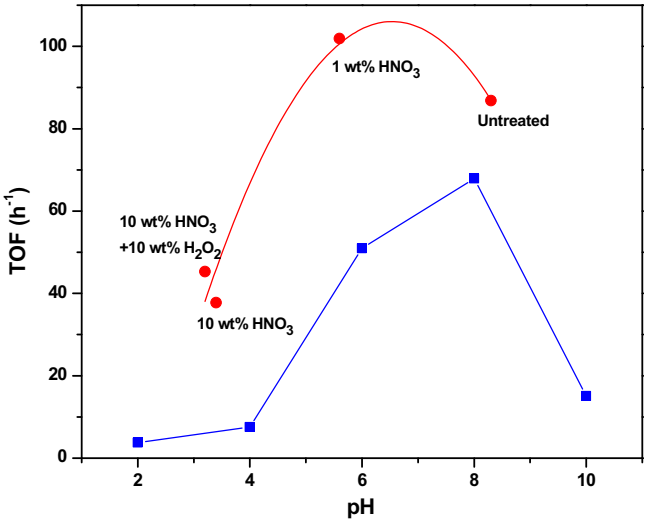

Fig. 15. The dependence of TOF on the pH of reaction medium; Pd/acid-treated activated carbon catalysts (●) and Pd/C (untreated) with pH control (■).

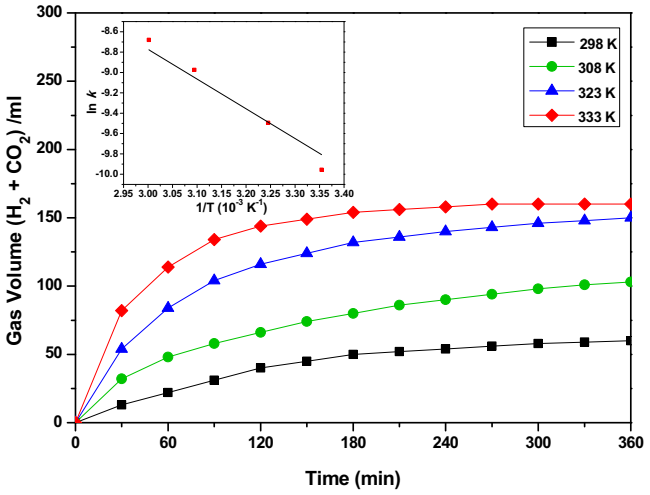

Fig. 16. Hydrogen-generating rate as a function of temperature in the formic acid dehydrogenation over 1 wt% HNO_3-treated Pd/C catalyst prepared by IR method (Inset represents Arrhenius plot of ln k vs. 1/T).

that the pH of the reaction medium was largely governed by the nature of the support. The pH of a solution containing untreated activated carbon and activated carbon treated with 1 wt% nitric acid was 8.3 and 5.6, respectively. However, the pH sharply dropped to 3.2 in the presence of the activated carbon treated with 10 wt% nitric acid, which may be due to the introduction of carboxylic acid groups on the surface. Fig. 15 clearly exhibits the volcano-type dependence of the catalytic activity on the pH of the reaction solution. The result implies that the catalytic activity is very sensitive to pH, and that neutral pH is a prerequisite to maximize the catalytic performance. To confirm the critical effect of the pH of the reaction solution, activity tests were carried out using the Pd/C (untreated) catalyst under different pH conditions. As shown in Fig. 15, a similar volcano-type relation between the TOF and the pH of the reaction solution was reproduced, which indicates that the pH determined by the functional groups of the support is of prime importance in achieving high catalytic performance. Instead of acetic or nitric acid, hydrochloric acid was used to adjust the pH in order to prevent any possible change in the surface functional groups, which may account for the different maximum points of these two volcano plots.

The unprecedented crucial role of the surface characteristics of a support in determining the catalytic performance may be rationalized from the mechanistic aspects of the reaction. From the viewpoint of the reaction mechanism, formic acid is first adsorbed on Pd the surface where a formate ion is formed by deprotonation. Then, the resulting palladium formate species may undergo β-hydride elimination to produce CO_2 and palladium hydride species. Finally, the recombination of the hydride species with a proton produces molecular hydrogen, and simultaneously Pd^0 is recovered. Under acidic conditions, the interaction between the acid sites of a support and the formic acid molecules may be beneficial to activate the formic acid molecules and to increase the surface concentration of formic acid [18]. However, high proton concentrations are unfavorable because the excess protons may promote recombination of the formate ion with a proton and/or retard the deprotonation step, which in turn may delay the decomposition of formate ions. Under basic conditions, on the other hand, the high concentration of OH^- ions in solution poses a problem in that competitive adsorption between the formate and hydroxyl ions may retard the catalysis cycle. It is worth noting that the unfavorable effect of OH^- ions on the reaction performance should be distinguished from the benign role of the weak amino groups. While the amino groups on the support may act as a proton scavenger and therefore facilitate formic acid dehydrogenation [19,20], the OH^- ions in solution may compete with the formate ions to occupy the adsorption sites. It was reported that formic acid oxidation is also strongly dependent on the presence of adsorbed anions [46]. Consequently, a neutral reaction medium is superior to an acidic or basic medium in providing a desirable environment for catalysis. In this regard, it can be concluded that tuning the nature of a support by achieving a balance between the two competitive aspects is very important to obtain high catalytic activity.

3.5. Effect of temperature on the reaction performance

To evaluate the rate dependence on the reaction temperature, a series of formic acid dehydrogenations using the 1 wt% HNO_3-treated Pd/C catalyst (**IR**) were carried out at different temperatures ranging from 298 to 333 K. As shown in Fig. 16, the catalytic performance strongly depended on the reaction temperature. The apparent activation energy was calculated based on the Arrhenius plot given in the inset of the figure. The estimated E_a was 30 kJ/mol, which is lower than the previous value obtained in the presence of Pd/C catalyst reported elsewhere [13].

3.6. Catalyst reusability test

The reusability of a catalyst was tested by performing repeated reaction cycles using the 1 wt% HNO_3-treated Pd/C catalyst (**IR**) under the same reaction conditions. At the end of a reaction cycle, the catalyst was isolated by filtration, washed thoroughly with water, dried at 383 K for 12 h, and then reused. As shown in Fig. 17, the catalytic activity was maintained without any apparent loss of activity after the third recycle run, which indicates that the catalytic activity can be almost fully recovered by drying at an elevated temperature. Chan and coworkers also reported that simple drying at an elevated temperature was efficient to regenerate Pd/C [13] or PtRuBiOx/C [55] catalyst, respectively.

4. Conclusion

A range of Pd/C catalysts were systematically prepared by adopting different methods; and applied for formic acid dehydrogenation under ambient conditions without additives. It was found that the physicochemical properties of the active metal as well as the sup-

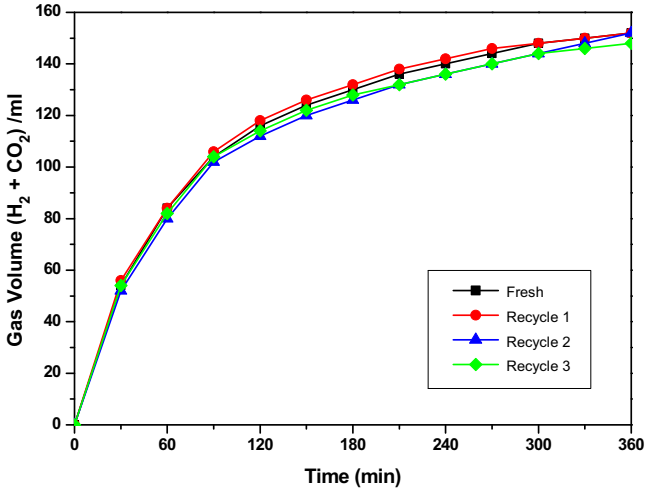

Fig. 17. Recycle runs of the formic acid dehydrogenation over 1 wt% HNO_3-treated Pd/C catalyst prepared by IR method.

port can be controlled by changing the catalyst preparation method, and that catalytic activity was strongly affected by the preparation method adopted. The observed volcano-shaped change in activity with respect to the Pd particle size clearly shows that the active metal size has a notable impact on the catalytic performance. The surface structure of Pd may be another factor to be considered, and a smaller [111]/[200] ratio is preferred. The electronic state of Pd also plays an important role in facilitating the reaction. While Pd^{2+} was totally ineffective, Pd^0 or the $Pd^0/Pd(OH)_2$ mixture effectively promoted the reaction. Moreover, the nature of the oxygen-containing groups on the activated carbon surface and their concentration exerted a large influence on the catalytic activity. The catalyst activity shows a strong volcano-type dependence on the pH of the reaction solution, which is determined by the functional groups of an acid-treated support. Thus, a neutral pH is favorable for accelerating the reaction. The unprecedented crucial role of the nature of the support may be explained by the following two factors: (i) recombination of the formate ion with a proton and/or delayed deprotonation by excess protons in an acidic solution and (ii) retardation of the catalysis cycle by competitive adsorption between the formate and hydroxyl ions in a basic solution. Therefore, controlling the nature of a support by balancing the two competitive factors is important to achieve high catalytic performance. The estimated apparent activation energy is 30 kJ/mol, which is lower than the previously reported value obtained when using Pd/C catalyst without additives. The catalyst could be recycled three times without any apparent loss of activity.

Acknowledgments

This research was supported by Basic Science Research Program through the National Research Foundation of Korea (NRF) funded by the Ministry of Education (2016R1D1A3B02006928).

References

[1] A. Boddien, H. Junge, Nat. Nanotechnol. 6 (2011) 265–266.
[2] M. Grasemann, G. Laurenczy, Energy Environ. Sci. 5 (2012) 8171–8181.
[3] Q.-L. Zhu, Q. Xu, Energy Environ. Sci. 8 (2015) 478–512.
[4] W.-W. Zhan, Q.-L. Zhu, Q. Xu, ACS Catal. 6 (2016) 6892–6905.
[5] T. Schaub, R.A. Paciello, Angew. Chem. Int. Ed. 50 (2011) 7278–7282.
[6] G.A. Filonenko, R. van Putten, E.N. Schulpen, E.J.M. Hensen, E.A. Pidko, ChemCatChem 6 (2014) 1526–1530.
[7] T.W. Myers, L.A. Berben, Chem. Sci. 5 (2014) 2771–2777.
[8] W.-H. Wang, M.Z. Ertem, S. Xu, N. Onishi, Y. Manaka, Y. Suna, H.e Kambayashi, J.T. Muckerman, E. Fujita, Y. Himeda, ACS Catal. 5 (2015) 5496–5504.
[9] K. Tedsree, T. Li, S. Jones, C.W.A. Chan, K.M.K. Yu, P.A.J. Bagot, E.A. Marquis, G.D.W. Smith, S.C.E. Tsang, Nat. Nanotechnol. 6 (2011) 302–307.
[10] Q.-L. Zhu, Q. Xu, Chemistry 1 (2016) 220–245.
[11] Z.-L. Wang, J.-M. Yan, H.-L. Wang, Y. Ping, Q. Jiang, Sci. Rep. 2 (2012) 598–603.
[12] M. Martis, K. Mori, K. Fujiwara, W.-S. Ahn, H. Yamashita, J. Phys. Chem. C 117 (2013) 22805–22810.
[13] C. Hu, J.K. Pulleri, S.-W. Ting, K.-Y. Chan, Int. J. Hydrogen Energy 39 (2014) 381–390.
[14] X. Wang, G.-W. Qi, C.-H. Tan, Y.-P. Li, J. Guo, X.-J. Pang, S.-Y. Zhang, Int. J. Hydrogen Energy 39 (2014) 837–843.
[15] Q.-L. Zhu, N. Tsumori, Q. Xu, Chem. Sci. 5 (2014) 195–199.
[16] F.-Z. Song, Q.-L. Zhu, N. Tsumori, Q. Xu, ACS Catal. 5 (2015) 5141–5144.
[17] M. Navlani-García, K. Mori, M. Wen, Y. Kuwahara, H. Yamashita, Bull. Chem. Soc. Jpn. 88 (2015) 1500–1502.
[18] M. Navlani-García, M. Martis, D. Lozano-Castelló, D. Cazorla-Amorós, K. Mori, H. Yamashita, Catal. Sci. Technol. 5 (2015) 364–371.
[19] A. Bulut, M. Yurderi, Y. Karatas, M. Zahmakiran, H. Kivrak, M. Gulcan, M. Kaya, Appl. Catal. B: Environ. 164 (2015) 324–333.
[20] K. Mori, M. Dojo, H. Yamashita, ACS Catal. 3 (2013) 1114–1119.
[21] H. Dai, N. Cao, L. Yang, J. Su, W. Luo, G. Cheng, J. Mater. Chem. A 2 (2014) 11060–11064.
[22] H. Dai, B. Xia, L. Wen, C. Du, J. Su, W. Luo, G. Cheng, Appl. Catal. B: Environ. 165 (2015) 57–62.
[23] L. Yang, X. Hua, J. Su, W. Luo, S. Chen, G. Cheng, Appl. Catal. B: Environ. 168–169 (2015) 423–428.
[24] C. Feng, Y. Hao, L. Zhang, N. Shang, S. Gao, Z. Wang, C. Wang, RSC Adv. 5 (2015) 39878–39883.
[25] S. Zhang, Ö. Metin, D. Su, S. Sun, Angew. Chem. Int. Ed. 52 (2013) 3681–3684.
[26] S.-T. Gao, W. Liu, C. Feng, N.-Z. Shang, C. Wang, Catal. Sci. Technol. 6 (2016) 869–874.
[27] X. Gu, Z.-H. Lu, H.-L. Jiang, T. Akita, Q. Xu, J. Am. Chem. Soc. 133 (2011) 11822–11825.
[28] Ö. Metin, X. Sun, S. Sun, Nanoscale 5 (2013) 910–912.
[29] M. Yurderi, A. Bulut, M. Zahmakiran, M. Kaya, Appl. Catal. B: Environ. 160–161 (2014) 514–524.
[30] M. Yurderi, A. Bulut, N. Caner, M. Celebi, M. Kaya, M. Zahmakiran, Chem. Commun. 51 (2015) 11417–11420.
[31] Z.-L. Wang, J.-M. Yan, Y. Ping, H.-L. Wang, W.-T. Zheng, Q. Jiang, Angew. Chem. Int. Ed. 52 (2013) 4406–4409.
[32] M.-H. Jin, D. Oh, J.-H. Park, C.-B. Lee, S.-W. Lee, J.-S. Park, K.-Y. Lee, D.-W. Lee, Sci. Rep. 6 (2016) 33502–33513.
[33] Y. Karatas, A. Bulut, M. Yurderi, I.E. Ertas, O. Alal, M. Gulcan, M. Celebi, H. Kivrak, M. Kaya, M. Zahmakiran, Appl. Catal. B: Environ. 180 (2016) 586–595.
[34] J.-M. Yan, Z.-L. Wang, L. Gu, S.-J. Li, H.-L. Wang, W.-T. Zheng, Q. Jiang, Adv. Energy Mater. 5 (2015) 1500107–1500112.
[35] A. Bulut, M. Yurderi, Y. Karatas, Z. Say, H. Kivrak, M. Kaya, M. Gulcan, E. Ozensoy, M. Zahmakiran, ACS Catal. 5 (2015) 6099–6110.
[36] Q.-L. Zhu, N. Tsumori, Q. Xu, J. Am. Chem. Soc. 137 (2015) 11743–11748.
[37] Y. Chen, Q.-L. Zhu, N. Tsumori, Q. Xu, J. Am. Chem. Soc. 137 (2015) 106–109.
[38] S. Domínguez-Domínguez, Á. Berenguer-Murcia, D. Cazorla-Amorós, Á. Linares-Solano, J. Catal. 243 (2006) 74–81.
[39] S.L. Goertzen, K.D. Thériault, A.M. Oickle, A.C. Tarasuk, Carbon 48 (2010) 1252–1261.
[40] V.A. Semikolenov, Russ. Chem. Rev. 61 (2) (1992) 168–174.
[41] J. Kim, Y.-M. Chung, S.-M. Kang, C.-H. Choi, B.-Y. Kim, Y.-T. Kwon, T.J. Kim, S.-H. Oh, C.-S. Lee, ACS Catal. 2 (2012) 1042–1048.
[42] G. Blanco-Brieva, E. Cano-Serrano, J.M. Campos-Martin, J.L.G. Fierro, Chem. Commun. (2004) 1184–1185.
[43] V. Climent, J.M. Feliu, J. Solid State Electrochem. 15 (2011) 1297–1315.
[44] J.V. Perales-Rondón, J. Solla-Gullón, E. Herrero, C.M. Sánchez-Sánchez, Appl. Catal. B: Environ. 201 (2017) 48–57.
[45] S.G. Sun, Y.Y. Yang, J. Electroanal. Chem. 467 (1999) 121–131.
[46] V. Grozovski, V. Climent, E. Herrero, J.M. Feliu, Phys. Chem. Chem. Phys. 12 (2010) 8822–8831.
[47] D.A. Bulushev, M. Zacharska, E.V. Shlyakhova, A.L. Chuvilin, Y. Guo, S. Beloshapkin, A.V. Okotrub, L.G. Bulusheva, ACS Catal. 6 (2016) 681–691.
[48] N. Patel, R. Fernandes, A. Miotello, J. Catal. 271 (2010) 315–324.
[49] M. Navlani-Garcia, K. Mori, A. Nozaki, Y. Kuwahara, H. Yamashita, Appl. Catal. A: Gen. 527 (2016) 45–52.
[50] M.L. Toebes, M.K. van der Lee, L.M. Tang, M.H.H. in't Veld, J.H. Bitter, A.J. van Dillen, K.P. de Jong, J. Phys. Chem. B 180 (2004) 11611–11619.
[51] E. Papirer, J. Dentzer, S. Li, J.B. Donnet, Carbon 29 (1991) 69–72.
[52] Y. Otake, R.G. Jenkins, Carbon 31 (1993) 109–121.
[53] P.E. Fanning, M.A. Vannice, Carbon 31 (1993) 721–730.
[54] J.L. Figueiredo, M.F.R. Pereira, M.M.A. Freitas, J.J.M. Órfão, Carbon 37 (1999) 1379–1389.
[55] C. Hu, S.-W. Ting, J. Tsui, K.-Y. Chan, Int. J. Hydrogen Energy 37 (2012) 6372–6380.